Marshall Plan Scholarship Paper

Oxidative and initiated Chemical Vapor Deposition for the Synthesis of Sulfonated Polymer Electrolyte Membranes

DIPL.-ING. PAUL CHRISTIAN

Massachusetts Institute of Technology

Feb 9th – Aug 31st 2017

Supervisors

PROF. KAREN K. GLEASON, PHD
Department of Chemical Engineering
Massachusetts Institute of Technology

ASS. PROF. DR. ANNA M. COCLITE
Institute of Solid State Physics
Graz University of Technology

Contents

Abstract

In this study, two solvent-free polymerization techniques, namely initiated and oxidative Chemical Vapor Deposition (iCVD and oCVD, respectively), were evaluated in their ability to produce polymer electrolyte membranes. While the iCVD technique allows the deposition of polymers with side-chain functionality by radical polymerization, the oCVD method enables the synthesis of polymers with backbone functionality. Vapor-based synthesis of poly(p-phenylene oxide) [PPO] was attempted by oCVD, employing different oxidants and co-evaporants under various experimental conditions. The findings demonstrate that a catalytic surface, a necessary precondition for the polymerization, can be formed on a substrate, but PPO was not obtained. On the other hand, poly(glycidyl methacrylate) [pGMA] films were successfully synthesized by iCVD, employing different cross-linkers and substrate materials. Post-deposition sulfonation was explored to turn samples into electrolytic materials. While delamination occurred from flat, rigid substrates like silicon, better adhesion was found on rough surfaces such as poly(ethylene terephthalate) or porous substrates such as nylon. Apart from chemical and morphological characterizations, also preliminary data on the conductivity of such films was obtained. The results show promising material properties, with conductivities above $\sigma > 10$ mS/cm. This motivates further studies of such vapor-synthesized, thin film polyelectrolyte membranes, in which also their implementation in applications such as biofuel cells or drug delivery is explored.

Introduction

Polymer electrolyte membranes (PEMs) are crucial components in applications like fuel cells (among others), facilitating selective (protonic) charge transport between the electrodes.[1–3] In addition to high protonic conductivities, these materials are required to withstand elevated temperatures as well as a harsh chemical environment.[3,4] These membranes are often composed of fluorinated parts providing the necessary stability and an acid group for ionic conductivity.[5] However, synthesis of such membranes is usually a tedious and costly process, especially as common solvents are often absent and process temperatures or interface control can become limiting factors.[6,7] Also, novel applications such as biofuel cells foster interest in alternative PEM concepts, often prepared directly on unconventional substrates such as paper.[8] The direct preparation of PEMs on more delicate supports puts additional restrictions on the synthesis processes, usually limiting the use of harsh chemical and thermal conditions. Conformal, low-temperature and solvent-free techniques could (at least) partially circumvent these issues while allowing the preparation of cheaper, better-performing and application-tailored polymers. Among vapor-based polymerization techniques, initiated and oxidative Chemical Vapor Deposition (iCVD and oCVD, respectively) have emerged as promising candidates for PEM synthesis. Both techniques translate the richness and versatility of synthetic organic chemistry into vapor-based processes while still offering the advantages of a conventional liquid phase synthesis. The iCVD technique was already successfully utilized in the synthesis of a copolymer membrane of methacrylic acid and a perfluorinated compound, which showed promising ionic conductivity at ambient temperature.[9,10] However, elevated temperatures led to a loss of mechanical stability, thus putting most practical applications (e.g. in fuel cells) in question. In addition, the (weak) carboxylic acid group tends to anhydride formation, which comes at the loss of its proton-donating functionality and renders the polymer useless as ionomer.[11] This motivates the use of different, stronger acid groups like sulfonic acid, which is also the conductive group in commercial Nafion, one of the most commonly employed membranes.[12] However, sulfonation cannot be done directly by the iCVD process which implies the need of a post-deposition modification. This can, for example, be achieved by the incorporation of aromatic phenyl rings into the copolymer, which can be sulfonated through electrophilic substitution.[5] Another option are ring-opening reactions of epoxide groups in which sulfonic acid groups are attached. Possible candidates are polymers

incorporating glycidyl methacrylate (GMA). Previous work on this material relied on radiation-induced grafting of GMA onto various substrates and a subsequent sulfonation step.[13,14] By the use of the iCVD technique, this tedious effort can be avoided and preparation of stable membranes should be directly possible.[15] While this should also raise the conductivity further and overcome the issue of anhydride formation, it does not help with other thermal issues which arise from the chemistry of the polymer backbone. The iCVD process is based on sidechain polymerization, which results (almost) exclusively in polymers with hydrocarbon backbones and functional moieties attached as pendant groups. As this backbone provides little stability against thermal or chemical influences, this can become a severe shortcoming in the synthesis of polymer electrolyte membranes; usually, PEMs are exposed to both a harsh chemical and thermal environment of temperatures of 80 °C and above. Polymers with aromatic backbones are interesting for application as proton conductive membranes, providing good thermal and chemical stability. Oxidative Chemical Vapor Deposition (oCVD), a state-of-the-art vapor phase polymerization technique developed by the Gleason group at MIT, allows for the synthesis of polymers with such a backbone functionality.[16–18] Most prominently, oCVD is used for the synthesis of poly(3,4-ethylenedioxythiophene), a conductive polymer better known as PEDOT.[19,20] However, the (electrical) conductivity of these materials poses an issue. Instead of allowing selective passage only for protons, the polymer would short-circuit the electrodes as well. For this reason, the conjugation along the backbone has to be broken, which can, for example, be facilitated by the inclusion of an ether bond. A possible candidate is poly(p-phenylene oxide), in short PPO, which is a promising starting material for various applications including the usage as PEM after sulfonation.[21] Using PPO as a starting material for post-deposition sulfonation, the aim was to achieve a polymer electrolyte membrane. This should yield a material with high ionic conductivity as well as thermal stability which could, for example, be used in fuel cell application. The high glass transition temperature (T_g ≈ 210 °C) combined with high mechanical and hydrolytic stability make this material particularly appealing.[22] In Figure 1, the proposed synthesis route for sulfonated PPO by the oCVD technique is illustrated.

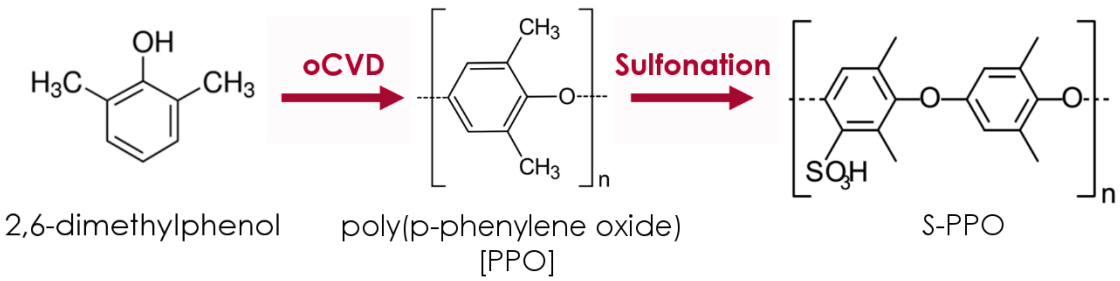

Figure 1. Proposed synthesis route for the preparation of an aromatic, sulfonated polymer via oCVD.

It should be emphasized that other polymer vapor deposition techniques such as iCVD do not allow the synthesis of such materials. Therefore, the oCVD technique can be regarded as complementing iCVD and extending the library of polymers available from vapor deposition.

In this study, oCVD and iCVD are evaluated for the synthesis of proton conductive membranes. For this, synthesis of PPO and pGMA co-polymers was attempted, with post-deposition sulfonation being used to introduce sulfonic acid functionalities to these starting materials. After synthesis, key material properties were analyzed utilizing techniques such as Fourier transform infrared spectroscopy (FT-IR) or electrochemical impedance spectroscopy (EIS). The FT-IR technique allows for chemical and compositional analysis after polymer synthesis and was used to evidence post-deposition material modifications (i.e. sulfonation). Impedance spectroscopy, on the other hand, was utilized to probe the electro-chemical properties of the films, most importantly the ionic conductivity. Sample characterization is complimented by structural/morphological analysis by scanning electron microscopy (SEM), optical and atomic force microscopy (AFM) as well as X-ray diffraction. This variety of analytical techniques allows to probe distinct key material properties during the different stages of membrane preparation, allowing for synthesis adjustments to be made more directly.

Fundamentals and Methods

In the following sections, a short introduction to important concepts of this work is given. The function of polymer electrolyte membranes is briefly discussed, followed by a description of the chemicals used and of the reaction mechanisms of polymer synthesis and sulfonation.

Polymer electrolyte membranes

The most common application of polymer electrolyte membranes (PEMs) are fuel cells, where they facilitate selective (ionic) charge transport. A graphical representation of such a system is provided in Scheme 1. The PEM is sandwiched between two electrodes through which working gases, for example hydrogen and oxygen, are flown. Assuming the ideal case of no gas cross-over, the gases can only react when the fuel is catalytically oxidized at the anode. While protons can move through the PEM, it does not allow for electron passage and they have to move through the electrical wires instead, which creates a current. Most PEMs facilitate the charge transport by incorporating strong acid groups, such as sulfonic acid, into their structure. When hydrated, protons dissociate from the acid groups and are transferred in the aqueous medium. Proton transport occurs then either by a hopping (Grotthuss mechanism) or vehicular mechanism.[23]

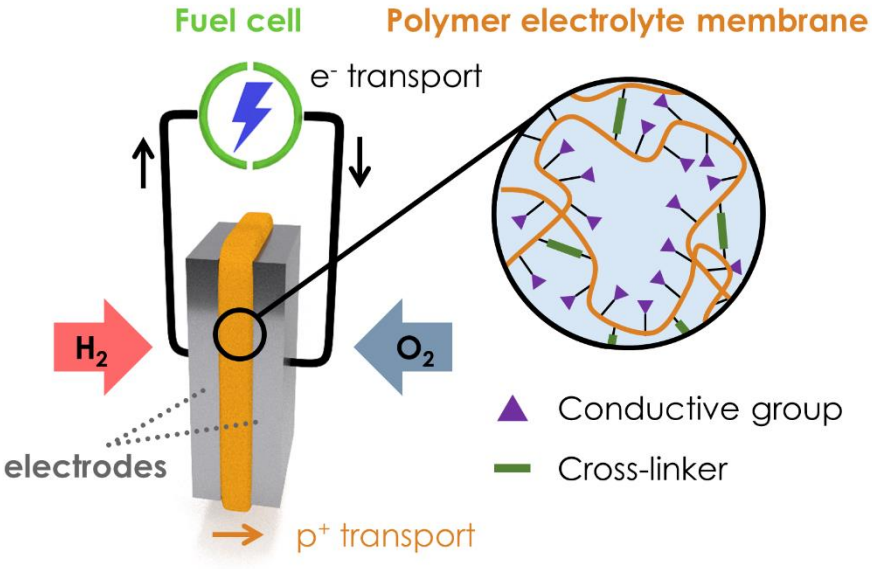

Scheme 1. Schematic representation of a polymer electrolyte fuel cell, depicting the membrane/electrode assembly. The ionic transport in the membrane is usually facilitated by conductive groups (e.g. acids groups such as sulfonic acid), which become conductive when hydrated. For improved stability (chemically & physically), a cross-linker can be employed.

Deposition techniques

In the following section, a short introduction to the two main deposition techniques used in this work is given. A more exhaustive description of these methods and of their working principles can be found in several comprehensive reviews.[16,24–26]

oxidative Chemical Vapor Deposition

Oxidative Chemical Vapor Deposition (oCVD) allows for material engineering where monomer units constitute the polymer backbone instead of being merely attached as functional side groups.[27] The technique relies (at least formally) on the deprotonation of the monomer build blocks after oxidation, which is facilitated by an oxidant like $Cu(II)Cl_2$ or $Fe(III)Cl_3$.[28] The process is carried out at lower pressures (typically a few Pa) and all reagents are delivered in vapor form, similar to the iCVD technique (for a schematic representation of the experimental setup, see Figure 2). A plethora of different chemistries are accessible with the oCVD technique. The building blocks are mostly aromatic compounds such as phenols, anilines or thiophene derivatives, meaning that the resulting polymers are often conjugated and thus conductive materials like PEDOT or polyaniline.[18]

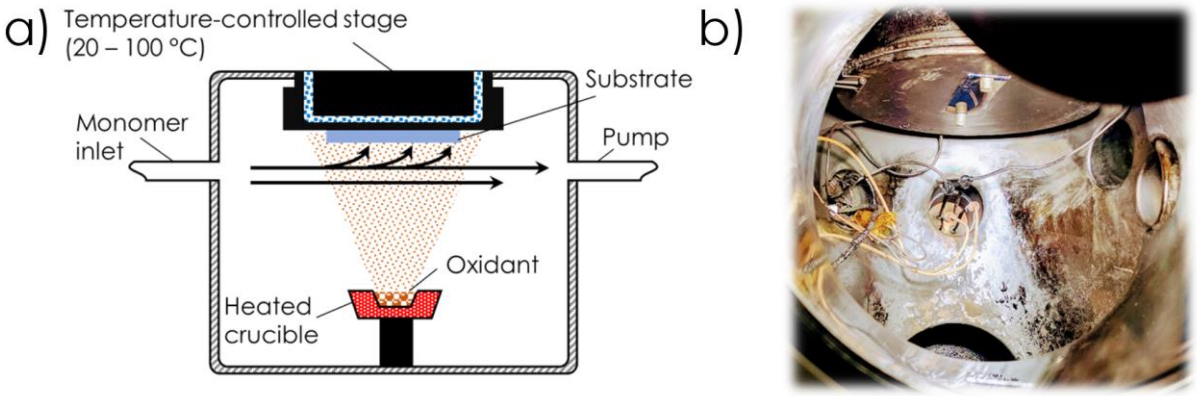

Figure 2. (a) Schematic of an oCVD setup, illustrating the deposition mechanism. An oxidant is delivered from a heated crucible to a substrate, where monomer is also adsorbed. On the surface, polymerization then proceeds by oxidative coupling. (b) The inside of an oCVD chamber, depicting electrical feedthroughs (left), sample stage with mounted sample (top) and monomer inlets (right).

initiated Chemical Vapor Deposition

This process follows in principle the steps of conventional radical polymerization in solution, except for the fact that all reagents are delivered from the gas phase. In Figure 3a, polymer deposition in an iCVD system is schematically depicted. Radicals are formed by thermal decomposition of an initiator (usually a peroxide) at a heated filament. These radicals then attack vinyl bonds of monomers absorbed at a substrate surface and, by subsequent monomer attachment, chain growth proceeds until terminated (either by a radical or another active chain).[25] The reaction equations for this mechanism are summarized in Figure 3b. All the polymerization reactions occur at the substrate interface, thus allowing for conformal coatings even on porous substrates or on surface structures with high aspect ratio.[29]

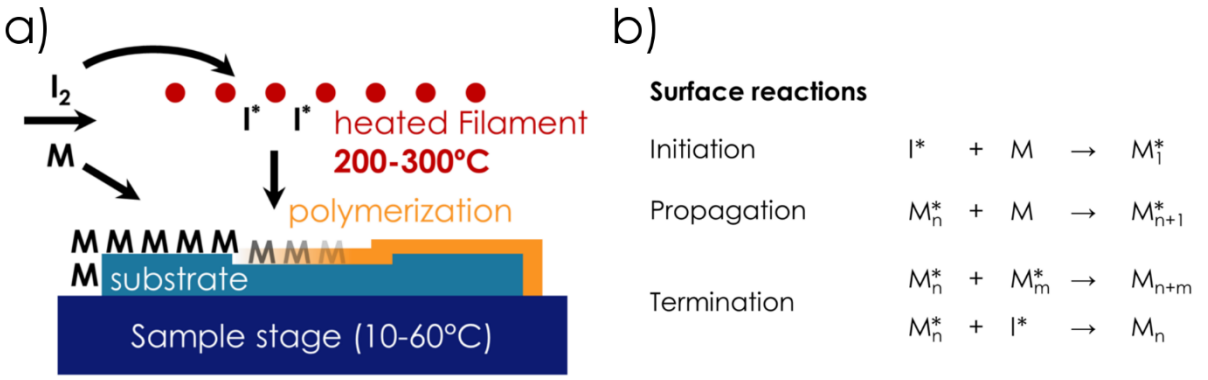

Figure 3. a) Schematic representation of the cross-section of an iCVD reactor, in which initiator molecules (I_2) are decomposed at a heated filament, yielding radicals I*. The radicals interact with monomer units (M) adsorbed on the surface, facilitating polymerization. b) Reaction mechanisms of the surface radical polymerization. Figures are adapted from literature.[30,31]

Materials and methods

For oCVD, 2,6-Dimethylphenol (2,6-DMP) was flown into a vacuum chamber from a heated jar. As oxidants, either iron chloride ($Fe(III)Cl_3$), cupric chloride ($Cu(II)Cl_2$) or cuprous chloride (Cu(I)Cl) were evaporated from a heated crucible. For some samples, pyridine was additionally flown into the reactor. The substrate temperature was kept at a set temperature by a heater/chiller system and the reactor body was also heated to a set temperature. A detailed description of the deposition parameters of the individual samples is provided in Table 1 (see Part I – oxidative Chemical Vapor Deposition).

Various co-polymers of glycidyl methacrylate (GMA) were prepared by iCVD in a custom build reactor. For this, three different cross-linkers and one co-monomer were

employed; divinylbenzene (DVB), Di(ethylene glycol) divinyl ether (DEGDVE), ethylene glycol dimethacrylate (EGDMA) and 1H,1H,2H,2H-Perfluorodecyl acrylate (PFDA), with their structural formulae being provided in Figure 4. The monomers were evaporated at different temperatures and flown into the reactor through a heated mixing line (held at 90 °C). For this, GMA, EGDMA and DVB were heated to 60 °C, PDFA to 70 °C and DEGDVE to 45 °C. The initiator, *tert*-butyl peroxide (TBPO), was then thermally decomposed at a resistively heated filament (Chromalloy O, Goodfellow). In order to obtain co-polymers with varying compositions, the flow rates of the reactants were adjusted by needle valves. For the initiator, a constant flow rate of 1 sccm was used. The reactor chamber is connected to a rotary vane pump and an automated butterfly valve is used to maintain the selected pressure of (26.6 ± 0.3) Pa during depositions. The substrate temperature was held at (40 ± 2) °C by a heater/chiller system (NESLAB) for most of the depositions. Only for p(GMA-DVB) films, the substrates were held at (27 ± 2) °C instead. All the chemicals were bought from Sigma-Aldrich.

As substrates, silicon wafers with a native oxide layer were used for most of the studies. For iCVD, samples were additionally prepared on commercial nylon membranes (Sterlitech, NY0214225, pore size 0.20 µm), poly(ethylene terephthalate) [PET] sheets or on porous Polytetrafluoroethylene membranes (PTFE, Goodfellow, pore size 0.45 µm).

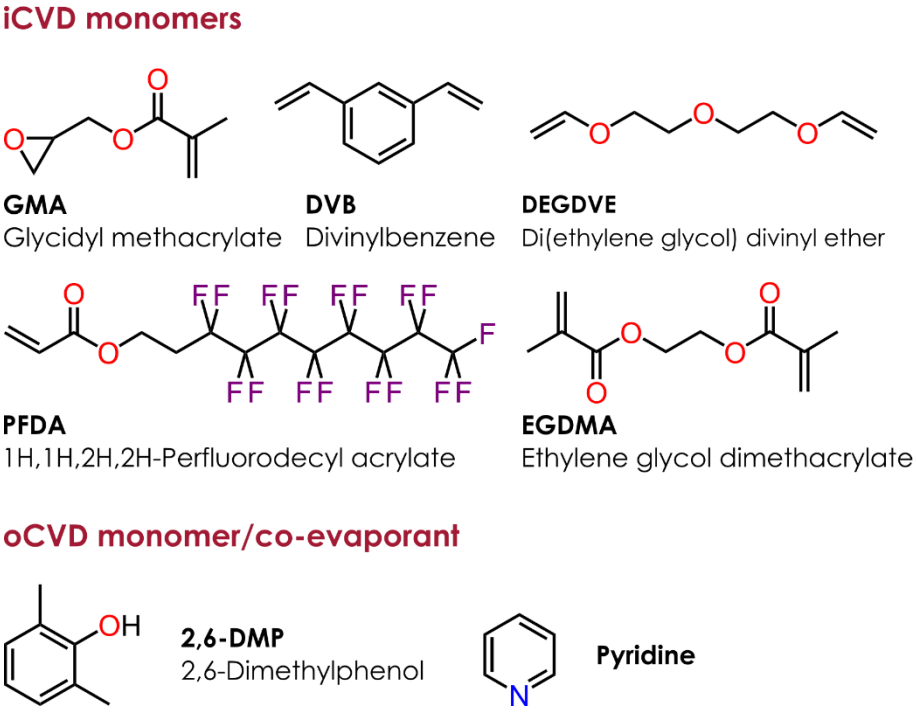

Figure 4. Chemical formulas of the monomers used in the iCVD and oCVD depositions of this study. The structures are labeled by their respective abbreviations (given in bold, capital letters), with their common names being stated below.

Sulfonation

Key components of a proton exchange membrane are the ionic groups which facilitate selective charge transfer. While various concepts are being explored in this context (e.g. the use protic ionic liquids[32]), commercial PEMs rely almost exclusively on sulfonated materials. The main advantage of sulfonated membranes over ones employing different acid groups (such as methacrylic acid[9,33] (MAA) or phosphonic acid[34]) is the higher performance. Strong acids (i.e. ones with a large acid dissociation constant K_a) deprotonate more easily in solution so that more protons become available for charge transport. However, a major drawback of sulfonated membranes is usually their challenging synthesis. The iCVD technique has been demonstrated in the past as a feasible method to (at least partially) circumvent these problems, albeit only membranes employing MAA were demonstrated so far.[9,10] To enhance the performance of such iCVD membranes further, it is desired to include sulfonic acid groups into the polymer. Unfortunately, this cannot be done in a single-step process; the iCVD method would require vinylsulfonic acid as a monomer, which tends to spontaneous polymerization and cannot be evaporated. Thus, a two-step process has to be used instead. First, iCVD is utilized to deposit a co-polymer film containing glycidyl methacrylate groups. In a second step, sulfonic acid groups are attached to these epoxide groups via a ring-opening reaction. This post-deposition reaction can be carried out under relatively mild conditions (80°C, nitrogen atmosphere), employing a water / isopropyl alcohol / sodium sulfite / sodium bisulfite mixture (weight ratio 77/10/10/3).[13] The reaction scheme is provided in Figure 5a, while the reaction setup is depicted in Figure 5b.

Compared to other sulfonation strategies, for example ones utilizing 1,3-Propane sultone,[35] this method offers two significant advantages. Firstly, the present sulfonation reaction employs relatively *small* chemicals, which modify only the epoxide end groups of the side chains. This should allow for a much better conversion efficiency when compared to the *bulkier* propane sultone, whose reaction also leads to a significantly prolonged polymer side chain. Secondly, the use of propane sultone raises several safety concerns as it is toxic, carcinogenic and mutagenic.[36] While similar safety concerns exist also for the glycidyl methacrylate monomer, it is considered much safer in its polymeric form pGMA. As the monomer is only employed in the closed environment of the iCVD reactor, this is less of an issue. However, it removes the need

of another vacuum system for the post-deposition sulfonation and all the reactions can be carried out under a fume hood with nitrogen purge instead.

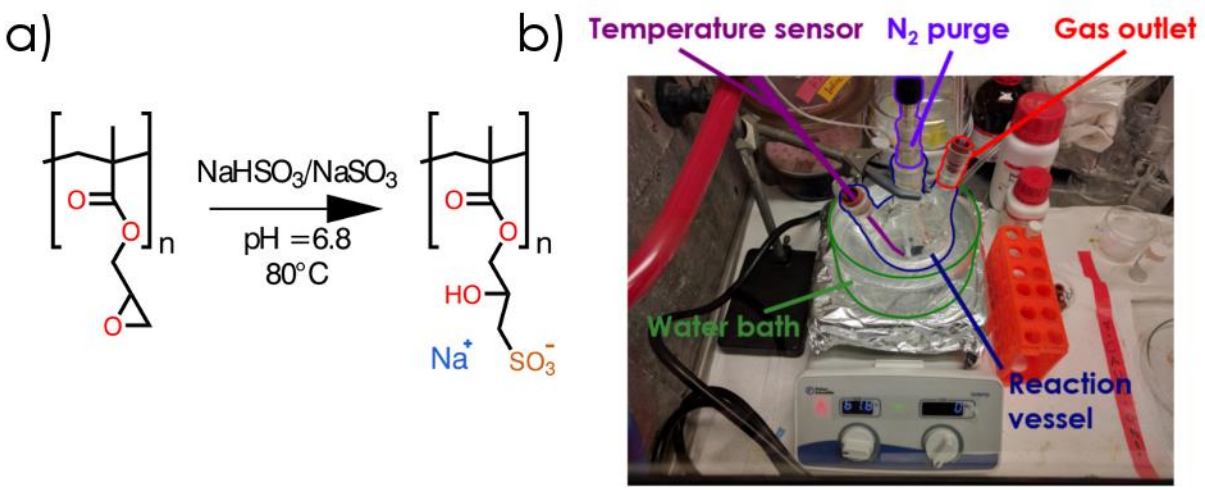

Figure 5. a) Reaction scheme depicting the ring opening sulfonation reaction of an epoxy group in a sodium sulfite/sodium bisulfite solution. b) Experimental sulfonation setup employing a three-neck round-bottom flask.

Experimental methods

Fourier Transform Infra-Red spectra (FT-IR) were collected on a Nicolet is50 spectrophotometer, equipped with a MCT detector, at a resolution of 4 cm^{-1}. Samples were measured either in transmission or in an attenuated total reflection (ATR) configuration, depending on the substrate. Experimental data are converted to absorbance and were automatically baseline corrected utilizing a custom *R* routine, implementing the *baseline* package.[37]

Atomic force microscopy (AFM) images were collected in tapping mode on a Nanosurf Easyscan 2 instrument, equipped with a PPP-NCLR-10 cantilever (Nanosensors). Data are leveled and corrected for artifacts in the freely available software package Gwyddion.[38]

Variable angle spectroscopic ellipsometry (VASE) was performed on a J.A. Woollam instrument. Data were collected at incidence angles of 65, 70, 75 ° for wavelengths in the range of 312 to 678 nm. Using Cauchy's equation to model the wavelength-dependent refractive index of the polymer, an optical model can be constructed. By fitting this model to the experimental data, thicknesses and optical constants of the polymeric films can be determined.

Specular X-ray diffraction (XRD) was carried out on a PANalytical Empyrean diffractometer, employing Cu Kα radiation (λ = 0.15418 nm). The system is equipped with a Göbbel mirror, various slits and a PIXcel^{3D} detector operated in scanning line mode. All data are converted to reciprocal space according to $|\overrightarrow{q_z}| = \frac{4\pi}{\lambda}\sin\theta$.

Scanning electron microscopy (SEM) images were recorded on a Hitachi TM3000 microscope, equipped with a Bruker Quantax 70 EDS detector. The acceleration voltage was either 5 kV or 15 kV, depending on the sample.

Electrochemical impedance spectroscopy (EIS) was performed on a Gamry Reference 600 potentiostat. Samples were characterized by four-point potentiostatic measurements. For this, samples were cut to size and inserted into a BekkTech BT-110 conductivity clamp. The clamp was then inserted into a sealed glass vessel, where it was exposed to a saturated water vapor atmosphere. Data were collected at 10 points per decade in the frequency range from 1 MHz to 0.1 Hz, applying an AC voltage of U_{RMS} = 10 mV. The experimental data were fitted to an equivalent circuit model for the frequency range from 10 kHz to 1 Hz, with data points close to the grid frequency (50 Hz) being removed prior evaluation. From the measured resistance R, the conductivity σ is then calculated according to $\sigma = l/(R \cdot w \cdot h)$, with l denoting electrode spacing and w, h being sample width and height (= thickness), respectively.

Experimental results and discussion

Vapor-phase synthesis of proton conductive polymers was attempted both by oCVD and iCVD. In the following sections, the experimental findings are presented and a short discussion of the results is provided.

Part I – oxidative Chemical Vapor Deposition

The polymerization of 2,6-Dimethylphenol to poly(p-phenylene oxide) was attempted by the oCVD technique. For this, different oxidants and experimental conditions were tested. The experimental parameters for selected depositions are summarized in Table 1. Please note that two different reactors were used in the experiments, with only one of them allowing for a flow rate determination.† Therefore, no flow rates are reported in Table 1.

Table 1. Experimental parameters for selected oCVD depositions. Oxidant (T_{ox}), substrate (T_{sub}), reactor body (T_{body}) and monomer temperatures (T_{mono}) are reported along working pressure (p). Marker (×) indicate the presence of the co-evaporant (pyridine).

Oxidant	T_{ox} [°C]	T_{sub} [°C]	T_{body} [°C]	T_{mono} [°C]	p [mTorr]	Pyridine [sccm]	Duration [hh:min]
$Fe(III)Cl_3$	250	55	70	60	15	-	1:10
	250	75	100	60	15	-	1:20
	250	100	140	60	15	-	2:00
$Cu(II)Cl_2$	>400	40	40	90	96	-	1:00
	>400	40	40	90	77	x	1:30
Cu(I)Cl	370	50	60	90	95	x	1:45

† Flow rates are commonly determined from the pressure increase in the reactor (minus the leak rate) when a gas flow is applied to the closed system. Depending on the volume of the chamber and position/type of the pressure sensor, however, certain gas flows might only yield a minor pressure increase and flow rates cannot be determined accurately in such cases.

Ferric chloride [Fe(III)Cl_3]

Polymerization of 2,6-DMP to PPO was attempted using ferric chloride as the oxidant. For this, different substrate temperatures typically employed in oCVD were tested. In Figure 6a, FT-IR spectra of the resulting samples are shown. All data feature several strong peaks, located at 1600, 3421 and 3479 cm^{-1}, respectively. This absorption pattern resembles closely that of ferric chloride (Figure 6b), meaning that the oxidant was just vapor-deposited on the substrate and no reaction occurred. In addition, spectra collected for samples prepared at higher substrate temperatures show sharp peaks at 1049, 1220 and 1379 cm^{-1}. These additional absorption peaks are likely due to unwanted contaminants. As the substrate temperature is increased, the reactor body temperature has to be raised as well. However, this also eases desorption from the reactor walls, which are usually covered by a mixture of oxidant(s) and monomer(s)/oligomers (cf. Figure 2b). While a clear identification was not possible, the pattern does neither match the absorption spectra of the 2,6-DMP monomer nor that of the PPO polymer.

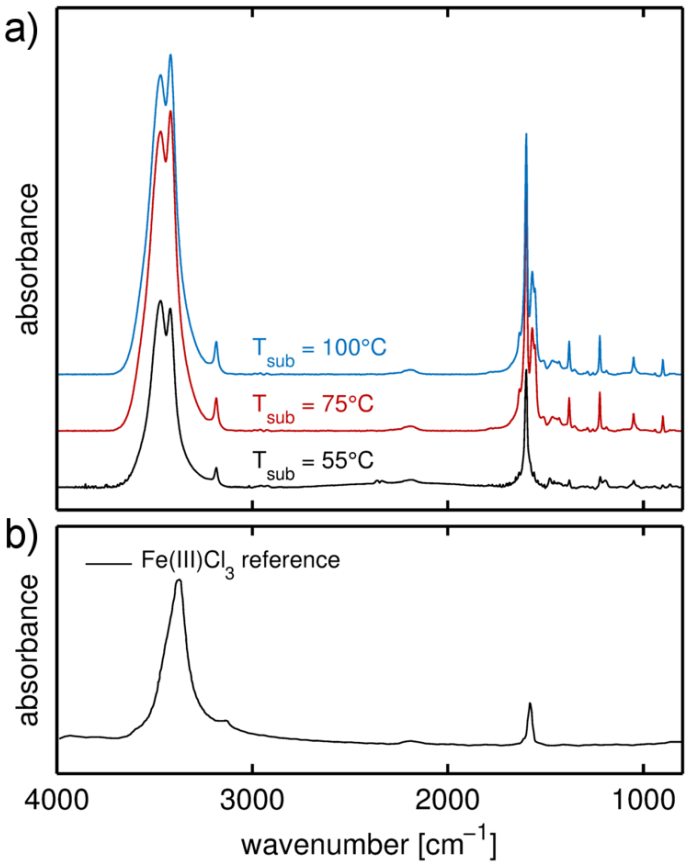

Figure 6. a) FT-IR spectra of three different samples prepared at different substrate temperatures. b) FT-IR spectra of ferric chloride taken from literature.[39] Data are shifted for clarity.

When pyridine is added to the process, morphology and chemical composition of the deposited films change, as evidenced by microscopy and FT-IR spectroscopy (data not shown). However, neither 2,6-DMP monomer nor PPO fractions are noted, indicating that polymerization cannot be performed by ferric chloride from the vapor phase (that is within the tested conditions). The addition of pyridine is motivated by the fact that the solution synthesis approach of PPO is preferably facilitated when a ligand is added, which in the case of PPO is usually pyridine.[40,41]

Cupric chloride [Cu(II)Cl_2]

As ferric chloride is substituted as oxidant by cupric chloride, FT-IR data remain inconclusive at first (data not shown). However, with the addition of pyridine to the process, a different behavior results. FT-IR data of such samples show a distinct absorption pattern which is identified as a coordination complex between cupric chloride and pyridine (*cf*. Figure 7). However, neither monomer nor polymer fractions are noted.

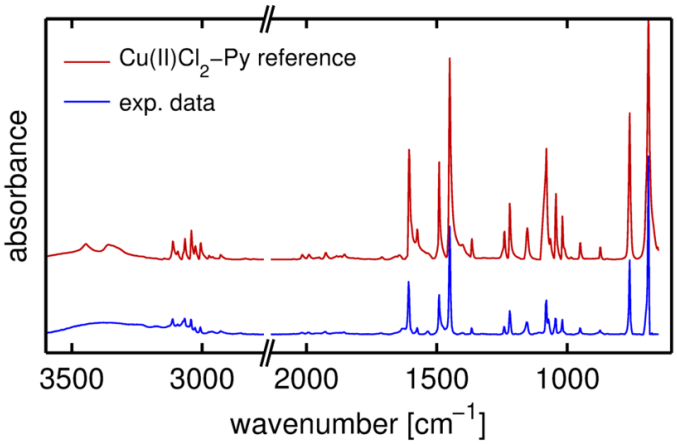

Figure 7. FT-IR spectra of a Cu(II)Cl_2-Pyridine coordination complex taken from a Thermo Scientific™ FTIR database (top) and experimental data from this study in comparison (bottom). Data are shifted for clarity.

An atomic force micrograph of such a sample reveals a micro-structured surface (*cf*. Figure 8a). The sample area is fully covered by small grains, exhibiting a mean radius of r = (635 ± 14) nm, as determined from the radial power spectral density function. The root-mean squared roughness is determined to σ_{RMS} = (99 ± 1) nm. Such a high roughness value is atypical for vapor-deposited films (on flat surfaces) as they are typically amorphous and (thus) conformal. Indeed, a XRD scan of such samples reveals distinct diffraction peaks, indicating the crystalline nature of the films (*cf*. Figure 8b). The experimental data are matched to the theoretical pattern of monoclinic

Cu(II)Cl_2-pyridine (CCDC Nr. PYRCUC02) by a database search, confirming the presence of the coordination complex.[42] The presence of unexplained peaks in the data shows that additional crystalline material is also present. As the FT-IR pattern did not evidence the presence of major contaminants (*cf*. Figure 7), it can be assumed that those peaks are also linked to cupric chloride and/or pyridine.

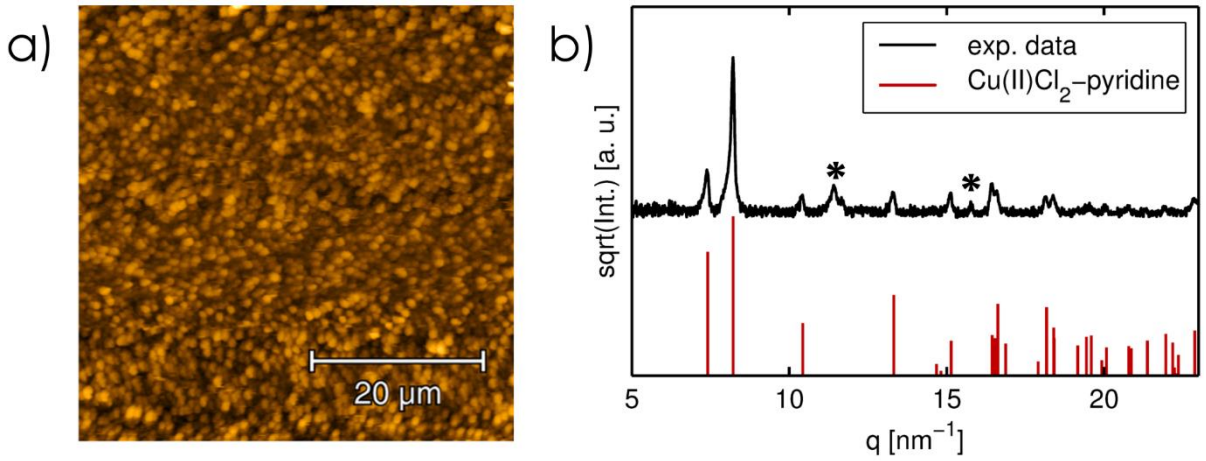

Figure 8. a) Atomic force micrograph of Cu(II)Cl_2-pyridine crystals. b) Experimental X-ray diffraction pattern of the sample and the matching theoretical pattern (CCDC Nr. PYRCUC02).[42] Bragg peaks which are not explained by the theoretical pattern are marked by an asterisk. Data have been background corrected and are reduced for noise.

Cuprous chloride [Cu(I)Cl]

When cuprous chloride is used instead of cupric oxide, little changes in the FT-IR spectra (*cf*. Figure 9). This indicates that also in this case a coordination complex is formed with pyridine, despite the difference in oxidation state of the involved oxidants. The main differences in the spectra are the presence of two additional broad absorption peaks, located at 1402 and 3226 cm^{-1}, respectively. Their position could hint at the presence of some material with –OH groups (such as the monomer), but other characteristic features of 2,6-DMP are absent. Therefore, it is assumed that also these peaks are related to contaminations stemming from the reactor walls. Again, experimental data do not show any PPO contribution.

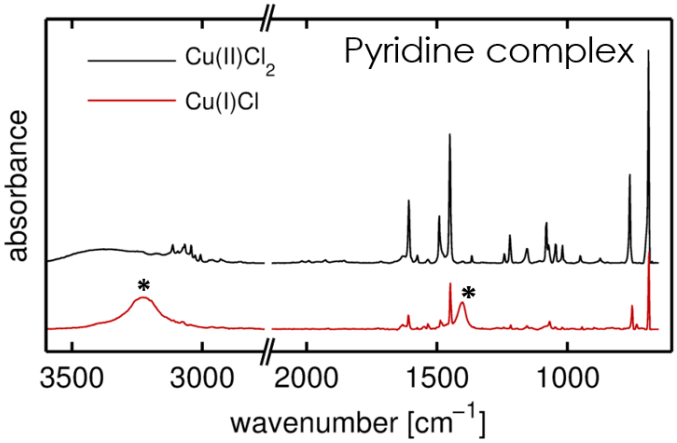

Figure 9. FT-IR spectra of samples prepared from either $Cu(II)Cl_2$ (top) or Cu(I)Cl oxidants (bottom). Both data sets evidence the formation of a coordinated complex with pyridine. However, in the case of cuprous chloride, additional absorption peaks are present in the spectrum (marked with asterisks). Data are shifted for clarity.

Discussion

The vapor-phase synthesis of poly(p-phenylene oxide) via oCVD was not accomplished within the experimental conditions tested. The data show that oxidants commonly employed in oCVD, such as ferric chloride, do not facilitate any polymerization reaction when the reactants are supplied from the vapor phase. Solution-based synthesis approaches have demonstrated in the past that the choice of oxidant and solvent have a strong impact on the reaction mechanism and kinetics. This means that a slightly unfavorable reactant combination might significantly slow down the polymerization or inhibit any reaction at all. Therefore, oCVD conditions were adapted to model the optimal conditions found for solution-based synthesis as closely as possible. Oxidants were switched to copper-based ones and pyridine vapor was supplied in addition to the reaction chamber. While even under those conditions no polymerization was observed, a coordinated-complex between the oxidant and pyridine was formed on the substrates, as evidenced by FT-IR data. This coordination complex is crucial for the polymerization reaction to occur in solution, indicating that either the absence of a solvent or too little interaction between the monomer and the surface prevent polymerization. A possible issue is the high vapor pressure of the monomer. It will easily desorb from any surface while the pressure is low and temperatures are high. However, higher temperatures are usually beneficial for chemical reactions to occur, while a low chamber pressure is required for the oxidant to reach the substrate. These opposing processes/material properties seem to be the main reason why the polymerization of 2,6-Dimethylphenol to poly(p-phenylene oxide) was not achievable in the current study and might not be feasible by oCVD in general.

Part II – initiated Chemical Vapor Deposition

In the following sections, the polymerization of GMA-containing films by iCVD and their subsequent sulfonation are discussed. Different strategies have been evaluated to improve mechanical stability of these materials during the sulfonation procedure. Also, some preliminary results on conductivity measurements of these films are presented.

pGMA synthesis and sulfonation

In a first step, GMA-containing polymer films were synthesized by iCVD on silicon substrates. Unless stated otherwise, films were usually deposited with a thickness of one micrometer. While the chosen film thickness is still well below that of commercial membranes (typically several tens of micrometers), it demonstrates that thicker films can also be prepared by iCVD. Further, proton transport properties can more reliably be analyzed for thicker films. To add (physical) stability to the polymers, DEGDVE was employed as a cross-linker in the polymerization. The resulting films were analyzed by FT-IR, an example is shown in Figure 10. The data demonstrate the successful polymerization of GMA by iCVD, matching the reference spectrum of pGMA almost exactly. This means that full functionality is being retained throughout the process and that vinyl bond conversion efficiency is high (as vinyl peaks, typically observed around 1630 and 990 cm^{-1}, are absent in the spectrum).[43] This means that monomer inclusion is likely low and also that both vinyl bonds of the cross-linker units are polymerized. However, this exact match with the pGMA homopolymer spectrum also evidences an issue. Due to the absence of chemical groups unique to the cross-linker, the co-polymer composition cannot be determined from the FT-IR data.

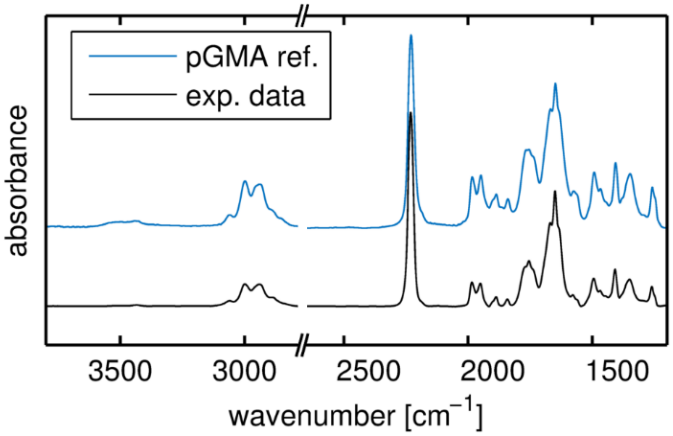

Figure 10. Experimental FT-IR spectrum of an as-prepared p(GMA-DEGDVE) polymer film (bottom) along the reference pattern of pGMA, taken from a Thermo Scientific™ FTIR database (top). Data are shifted for clarity.

In a next step, the p(GMA-DEGDVE) films were sulfonated in solution according to the procedure described in the section Sulfonation. In Figure 11, exemplary results for post-sulfonation polymer films are shown. The sample has been exposed to the reactant solution for six hours while being held at 70 °C. During the reaction, the polymer film had delaminated, an issue commonly encountered in the sulfonation process. While as-prepared films cover smoothly the silicon wafer surface, films would delaminate and fragment during the sulfonation (compare the photographs in Figure 11a). Picking up larger fragments and drying them on a silicon support, further analysis was possible. An AFM micrograph (in Figure 11b) reveals a rough surface area (σ_{RMS} = (13 ± 1) nm), which is in stark contrast to the smooth surface of as-prepared films (roughness approx. 1 nm, data not shown).

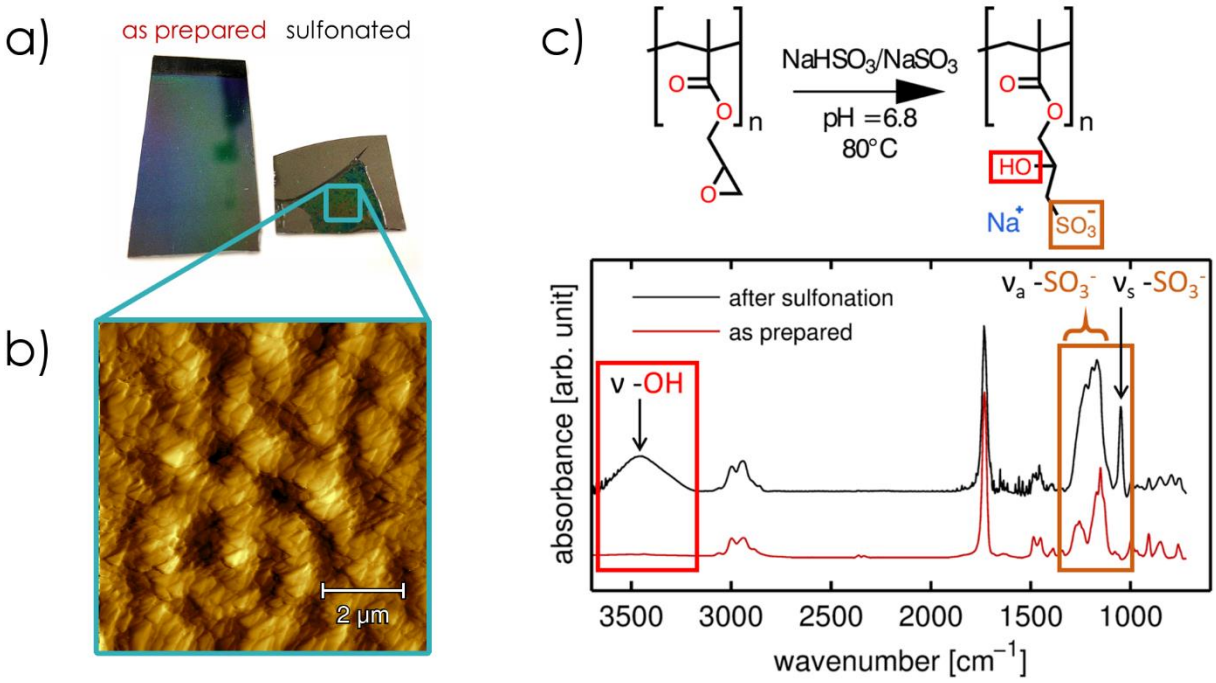

Figure 11. a) Photographs of an as-prepared p(GMA-DEGDVE) film on a silicon substrate and a delaminated piece after sulfonation (supported on silicon). b) AFM micrograph of the sulfonated polymer piece. c) Scheme depicting the chemical modification of GMA during sulfonation (top) and FT-IR spectra of the two samples (bottom), evidencing differences in chemical composition after the solution treatment. Data are shifted for clarity.

Film delamination and the changed surface structure indicate already that some modification has occurred in the film, which is confirmed in the chemical analysis by FT-IR (Figure 11c). The experimental spectra before and after sulfonation show clear differences in the fingerprint regions (1500-500 cm^{-1}) and in the –OH stretch regions (3600-3100 cm^{-1}). Post-sulfonation, the spectrum features peaks characteristic for

sulfonate groups, located at 1193 and 1047 cm^{-1}, as well as a broad absorption peak at 3446 cm^{-1}, attributed to the formation of hydroxide groups.[44] A comparison with the reaction scheme (Figure 11c, top) shows that the occurrence of these groups is associated with a successful opening of the epoxide so that the sodium salt of the sulfonic acid is then attached in a nucleophilic attack. While this means that iCVD-deposited GMA polymers can successfully be sulfonated, film delamination and subsequent fragmentation pose a serious challenge for any practical application. For this reason, one has to understand the occurrence of delamination first. From the experimental data, the change in hydrophilicity during sulfonation is identified as the most probable cause; as the sulfonic acid salt attaches, polymers become strongly hydrophilic and thus start swelling in the sulfonation medium, which in turn causes stress at the polymer/substrate interface. The rigid silicon substrate does not support the strong expansion of the polymer during swelling and thus, delamination occurs. It should be noted that, in principle, delamination could also be due to a too low cross-linking degree. For polymers deposited by iCVD, stable films are usually obtained at cross-linker fractions of about 10 % or above. However, varying monomer to cross-linker flow rates did not result in any stable films during sulfonation, while the same films were found stable in water at the same temperatures (data not shown). However, as DEGDVE content could not be determined from FT-IR data, no conclusive assessment of the cross-linker fraction could be made (however, successful cross-linking is evident from improved stability in water). Therefore, the following section will provide some examples of other co-monomers tested as well as other strategies to limit delamination during the sulfonation.

GMA-polymers with different co-monomers

A major advantage of the iCVD technique over other polymerization techniques is how easily polymers with different co-monomers can be synthesized, as the need for common solvents is absent. As it was not possible to detect DEGDVE fractions from FT-IR data and film delamination remained a critical issue independent of the tested deposition parameters, different co-monomers were investigated instead. For this, two other cross-linkers, DVB and EGDMA, as well as PFDA, a perfluorinated co-monomer, were tested. As their chemistry shows at least some differences to GMA (*cf*. Figure 4), their volume fraction can more easily be assessed from FT-IR data. Selected examples are provided in Figure 12, where experimental data are evaluated as a linear combination of the homopolymer spectra, weighted by their respective fraction and

normalized by the sample thickness. From a fit to the data, the composition is then evaluated. For GMA co-polymers with PFDA and EGDMA, reasonably good agreement is achieved (*cf*. Figure 12a,c,d). The fits match closely the experimental data and different GMA content can be distinguished (*cf*. Figure 12c,d). While this treatment can also be applied to p(GMA-DVB) polymers (*cf*. Figure 12b), the spectra show strong deviations from the fit in the fingerprint region (marked by an asterisk in the plot). The assumptions of little interaction between the co-monomers does not hold in this case and the co-polymer gives rise to additional absorption peaks. However, when the evaluated data range is reduced to the region of C-H stretch above 2800 cm^{-1}, polymer composition can still be determined by this routine. A more detailed description of this method and its limitations can be found in literature.[45]

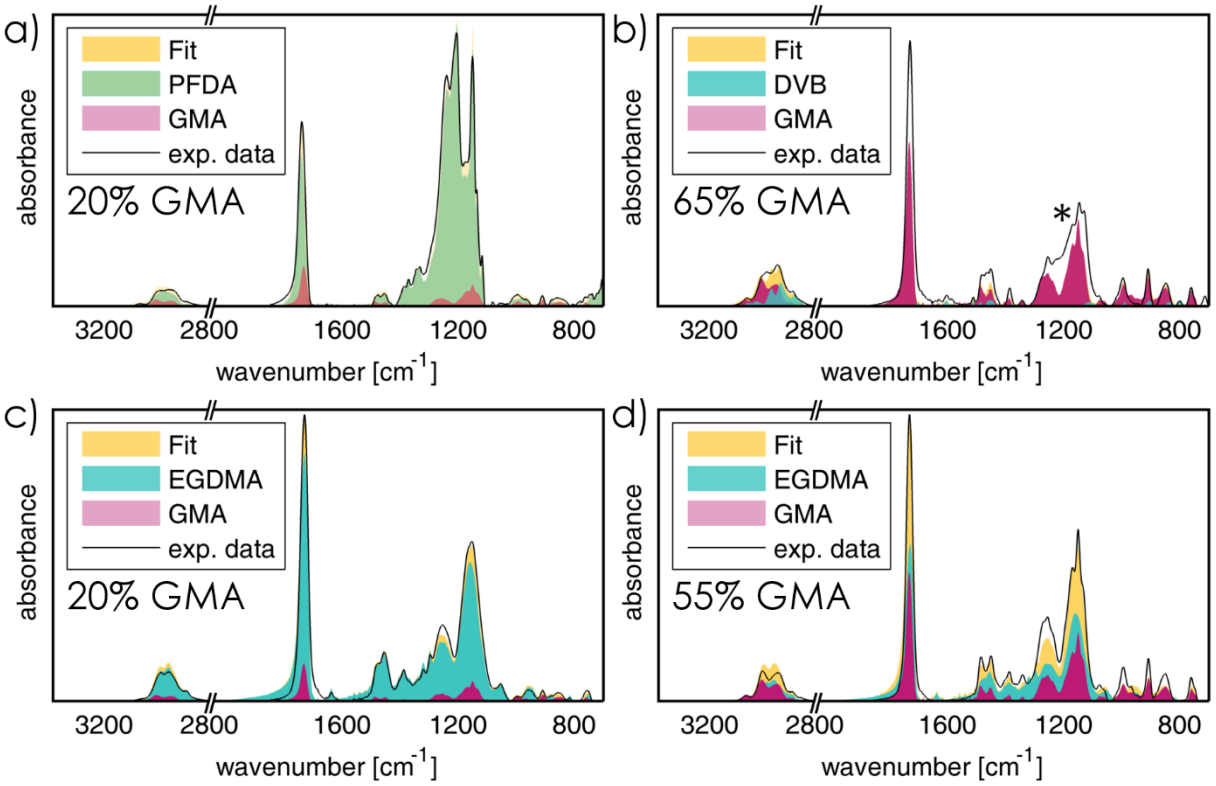

Figure 12. Exemplary FT-IR spectra of different GMA copolymers: a) p(GMA-PFDA), b) p(GMA-DVB) and c,d) p(GMA-EGDMA) films with different GMA content. For compositional analysis, experimental data are fitted by a linear combination of the respective homopolymer spectra. In case of the p(GMA-DVB) films, deviations from this model are noted (marked by an asterisk, see text for a more detailed explanation). Please note that so-determined volume fractions will have an absolute error of about 10 %, as there is a high degree of freedom in the baseline corrections.

While changing the co-monomer in the GMA films did allow for an easier compositional analysis, structural damage and delamination during sulfonation remained critical issues. Exemplary, optical micrographs of a p(GMA-PDFA) film and a p(GMA-DVB) film, after being exposed to the sulfonation solution, are shown in Figure 13a and b, respectively. Despite the high PFDA content (>90 %), ruptures and partial delamination occurred. For this reason, PFDA was not further considered. Likewise, DVB co-polymers were severely affected by the sulfonation process (Figure 13b). However, in contrast to PFDA, these samples exhibit a behavior more similar to that of p(GMA-DEGDVE) films. Interestingly, defined patterns are also noted on the samples, possibly hinting at the occurrence of phase separation in these films. Likewise, EGDMA films exhibit comparable behavior but also do not limit delamination (data not shown). While all the tested cross-linker seem to be feasible per se, altered chemistry does not limit delamination and thus, other strategies were evaluated instead.

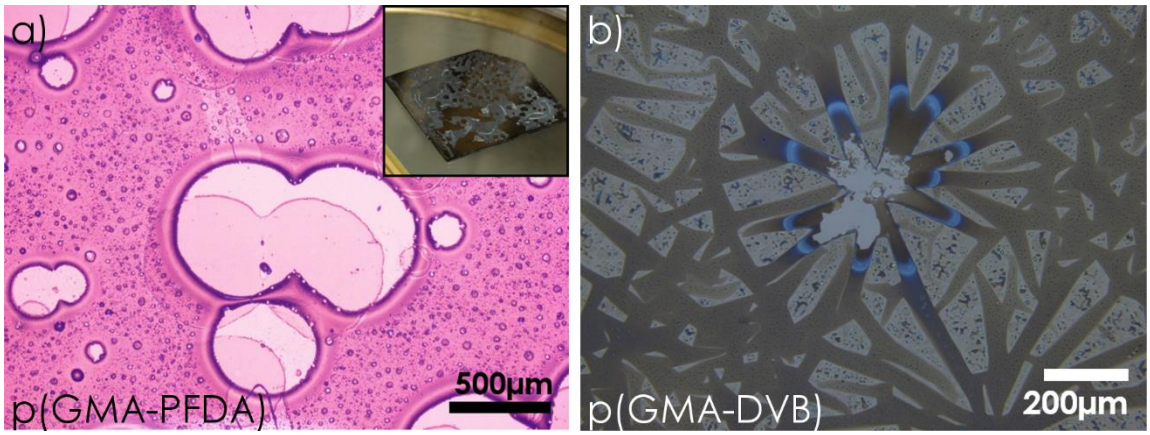

Figure 13. Optical microscopy images of samples after sulfonation: a) p(GMA-PFDA) film with little GMA content (<10 %), the inset depicting the entire sample. b) p(GMA-DVB) film with 60 % GMA content.

Grafting was explored as another possible strategy to cope with the delamination problem. For this, vinyltrichlorosilane (VTCS) was evaporated on silicon substrates in a vacuum oven held at 60°C. This procedure creates vinyl bonds on the surface, which can then be used to facilitate chemical links between the substrate and the polymer during the iCVD process. While ellipsometric data evidenced the formation of a thin silane layer on the substrate surface, the grafting did not result in a notable stability improvement (an example is shown in Figure 14). While grafting is usually a viable strategy to chemically bond thin films onto substrates, it cannot fully compensate for all the stress caused by the swelling of the micron-thick polymer during sulfonation. For

this reason, grafting was not further considered in this study and the focus was put on evaluating different substrates instead.

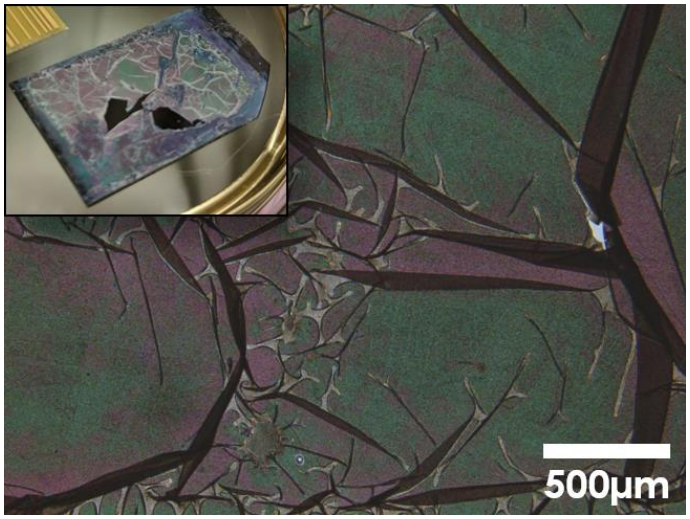

Figure 14. Optical microscopy image of a p(GMA-DEGDVE) sample prepared on a grafted substrate after sulfonation. The film exhibits partial ablation as well as strong creasing. The inset shows a photograph of the entire sample.

Nylon and PET substrates

While different cross-linkers, polymer compositions and also grafting was explored as possible ways to limit film delamination from silicon substrates during sulfonation, none of the evaluated strategies did result in a significant improvement. Therefore, also different substrates were evaluated for the preparation of sulfonated PEMs by iCVD. Two porous (nylon and PTFE) and a non-porous substrate (PET) were employed in the film preparation. From a material characterization point of view, the PET substrate offers the advantage of being more accessible to most of the analytical techniques employed in this study. Most importantly, FT-IR analysis can be performed in this case by using the surface-sensitive ATR configuration. As this requires substrate and polymer to be separated by a sharp interface, porous substrates are not well suited. For this reason, chemical analysis was performed exclusively on samples prepared on PET substrates. However, the porous substrates provide better stability to the iCVD polymers due to their larger surface area. Also, the porosity of the substrates eases water uptake, a possible advantage in the conductivity measurements.

Films prepared on either of these flexible substrates showed improved stability of the iCVD films during sulfonation. Exemplarily, FT-IR data of p(GMA-DEGDVE) samples are provide in Figure 15a, evidencing the differences in the measured spectra depending on the substrate choice (silicon or PET). Despite having an iCVD layer of about 1.5 µm

atop, the substrate is also partially sampled in the ATR measurement. However, the differences do not significantly alter the overall pattern and the iCVD polymer is easily recognized. After being kept in the sulfonation solution for 8 hours at 75 °C, the film remained attached to the substrate surface and FT-IR data evidence the successful conversion of the GMA groups (compare Figure 15b with the data in Figure 11c). While it should be noted that some samples also delaminated from PET (mostly when handled in a highly swollen state, e.g. during rinsing), overall stability was significantly improved in comparison to samples prepared on silicon.

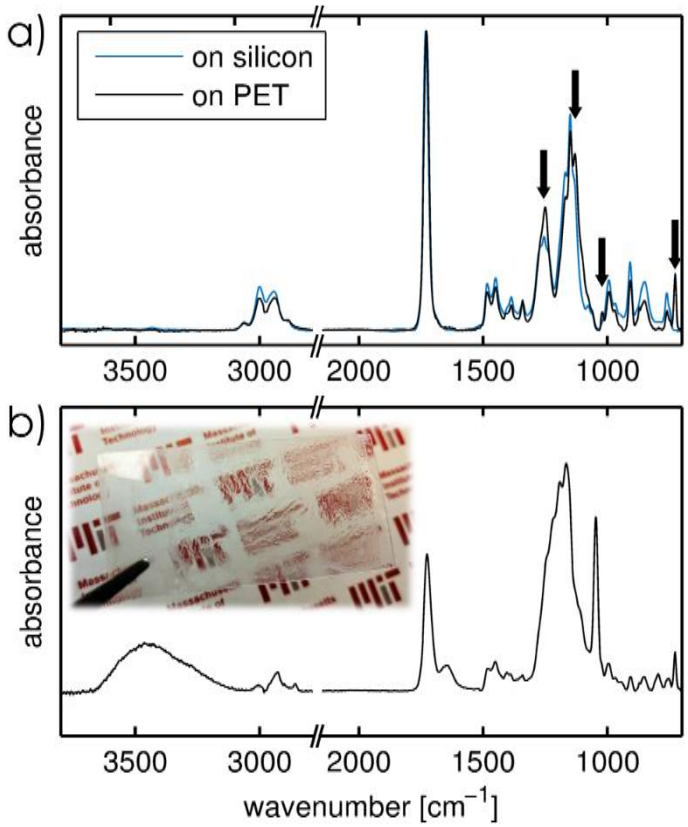

Figure 15. a) FT-IR spectra of as-prepared p(GMA-DEGDVE), prepared either on a silicon or on a PET substrate. The data are collected in transmission for silicon and in ATR configuration for PET. Arrows mark absorption peaks stemming from the PET substrate. b) FT-IR ATR spectrum of a sulfonated p(GMA-DEGDVE) sample on a PET substrate (8 hours at 75 °C). The inset depicts a photograph of the sample in the swollen state. While the left side of the transparent PET substrate has been left uncoated, strong wrinkling of the swollen iCVD polymer, covering the right part of the substrate, results in the image being *blurred out*. Data have been baseline and ATR-corrected (where applicable).

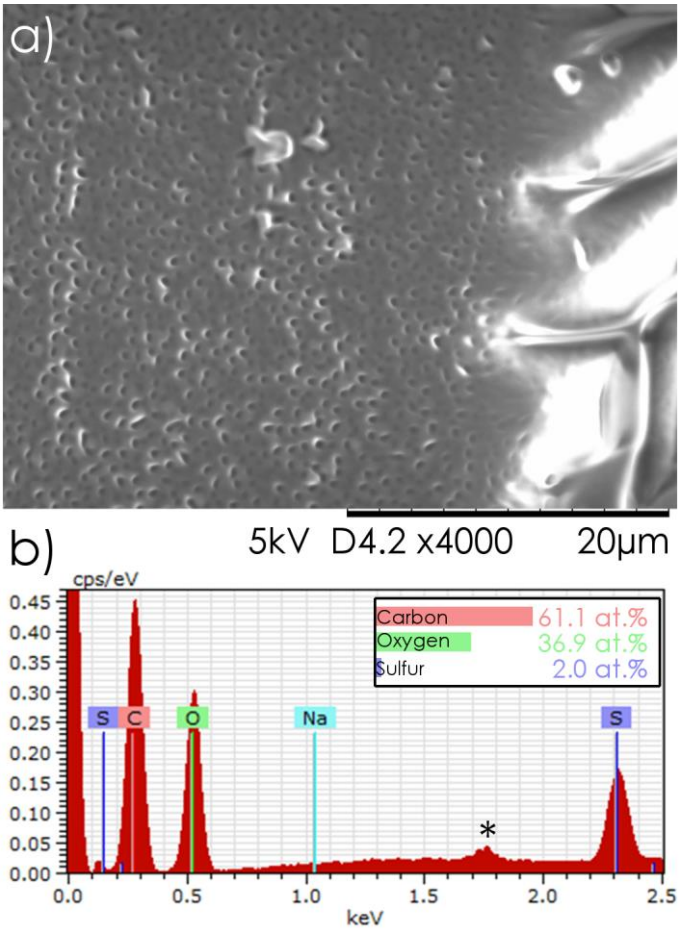

Figure 16. a) SEM image of a p(GMA-DEGDVE) coating on a PET substrate after sulfonation and ion exchange in 1 M sulfuric acid. b) EDX spectrum of the sample, evidencing the successful conversion of the salt to the acid state (as sodium is not detected). The inset shows a quantitative compositional analysis of the spectrum. Peaks stemming from a silicon powder contamination are indicated by an asterisk.

In another step, the transfer of the acid salt to sulfonic acid was tested. For this, samples were stored in one molar sulfuric acid for 8 hours, which should lead to a hydrolysis reaction. As exposure to a strong acid like sulfuric acid can have unwanted side-effects on the film/substrate, SEM images were taken after the reaction. Figure 16a shows an exemplary image of a p(GMA-DEGDVE) sample after acid exposure. Aside from strong charging effects due to the non-conductive substrate (bright areas in the image), the surface is covered with small dot-like features. Likely, the acid treatment had led to the formation of holes in the iCVD film. The EDX spectrum of this sample (Figure 16b) shows the absence of sodium (Na) while sulfur is still present, indicating a successful conversion of the film. A quantitative analysis of the spectrum yields a sulfur fraction of 2 % (see inset). From this data, a rough estimate about the sulfonation

conversion efficiency can be made. Assuming a GMA homopolymer (as it was not possible to determine the DEGDVE content), the carbon/oxygen/sulfur ratios would yield a conversion rate of about 40 %. However, this value is likely only a lower limit; as the EDX spectrum probes most of the sample thickness, carbon and oxygen content will also show some contribution from the PET substrate as well as from carbon contamination.

Conductivity measurements

Polymer electrolyte membranes are commonly tested either directly in fuel cell systems or separately in a conductivity cell. However, this requires rather thick polymer films (with tens of micrometers in thickness), which are not feasible to deposit with a research iCVD reactor. For this reason, thinner films are usually investigated instead, requiring more specialized experimental setups. As iCVD polymers can easily be prepared on different surfaces, this raises an interesting option: instead of preparing free-standing films, which are then contacted mechanically by the measurement electrodes, one can directly deposit the polymers on an electrode array. In this context, printed circuit boards (PCBs) are an interesting option as they are highly customizable and are cheaply available (an example is shown in the inset of Figure 17a). Electrodes with a varying spacing allow for conductivity measurements as a function of electrode separation distance, which can be useful to detect the influence of local defects (as they interfere with the otherwise linear relationship according to Ohm's law). Also, from the rough, polymeric substrate of the PCB one can expect improved adhesion between iCVD film and PCB, thus minimizing the delamination problem. While this was confirmed in the sulfonation experiments (data not shown), another issue arose during measurements. For this, samples are usually inserted into water, in order to hydrate the sulfonated films prior measurement (*cf*. Figure 17b). However, measurements turned out to be surprisingly unstable (data not shown). SEM images of repeatedly water-exposed samples revealed structural damage at the polymer-electrode interfaces (*cf*. Figure 17a). The gold-coated copper electrodes have a height of about 30 µm, which is much larger than the polymer thickness (approx. 1 µm). This difference makes the so important interface susceptible for defects, the SEM image showing creasing and ruptures in the iCVD layer on top of the electrodes (marked by arrows).

To avoid this issue, thin gold electrodes were evaporated on PET substrates instead (*cf*. Figure 17c). These electrodes had a thickness of just 50 nm and retained the

advantages of using a flexible substrate. For measurements, electrodes feature broader pads at their top, at which they can be connected by toothless alligator clips (*cf*. Figure 17d). While this concept did function in principle, the tedious and costly preparation process makes also this approach not feasible for evaluating a wider spectrum of samples. Thus, these thin gold electrodes were used only complementary to measurements with the BekkTech conductivity cell. In addition, samples were swollen in humidity rather than inserting them directly into water, allowing more time for the swelling process and also allowing the study of the time-dependence of the conductivity during water uptake.

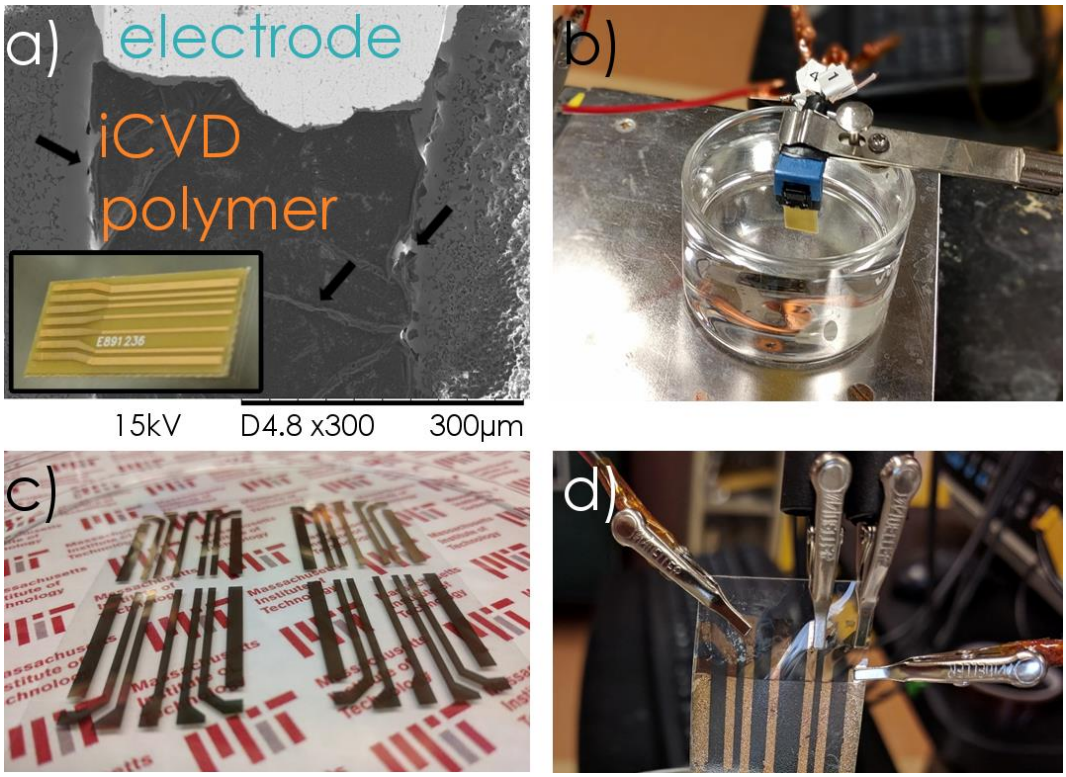

Figure 17. a) SEM image of the electrode-polymer interface on a PCB after sulfonation. The inset depicts a photograph of the full PCB, with an iCVD film covering the right part of the board. Arrows mark several defects at the polymer/electrode interface. b) EIS measurement setup in water. c) Gold electrodes evaporated on PET substrates. d) 4-point EIS measurement of a sulfonated iCVD film prepared on a PET substrate with a gold electrode array.

In the following, some preliminary conductivity data are presented for samples measured in humidity. As samples were prepared on nylon substrates, the uncoated substrate was investigated first. In order to exclude any influence of the post-deposition sulfonation reaction, the nylon substrate was put in the solution for 14 hours at 75 °C. In Figure 18a, changes in nylon conductivity as a function of time are

depicted, as determined from electrochemical impedance spectroscopy measurements in saturated humidity. While the sample does show some increase in conductivity over time (as the nylon substrate takes up water), the nylon remains overall highly resistive. This is a good indication that the nylon substrate was not strongly affected by the sulfonation process, allowing coating and substrate to be distinguished in the EIS measurements. In Figure 18b, the Nyquist plot of a representative impedance spectrum is shown (i.e. x- and y-axis depict the real and imaginary part of the impedance, respectively). The data feature most prominently a semicircle, corresponding to an equivalent circuit of a capacitance and a resistance in parallel. For practical reasons, an imperfect capacitance is usually considered, modeled by a constant phase element (CPE). While there is another, smaller semicircle noted at higher Z_{real} values, it can be neglected in the data evaluation; the membrane conductivity is calculated from the measured resistance, i.e. the intersection with the x-axis.

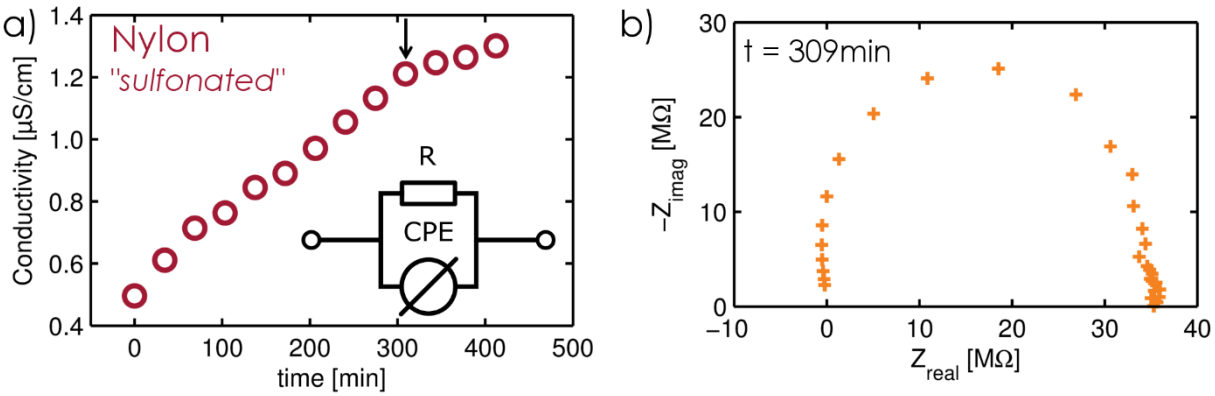

Figure 18. a) Changes in ionic conductivity for an uncoated nylon membrane, which was kept in the sulfonation reaction solution for 14 hours (at 75 °C) prior measurement. b) Nyquist plot depicting the impedance spectrum for a selected data point (marked with an arrow in a) The data were collected in a closed system at saturated humidity.

When evaluating sulfonated iCVD polymers deposited on nylon, a different behavior is observed. Impedance spectra for a p(GMA-EGDMA) film with 55 % GMA content (*cf*. Figure 12 for the FT-IR data) show a pronounced inductive behavior at high frequencies (above 10 kHz), which transits into a resistive/capacitive behavior at lower frequencies (for an exemplary data set, *cf*. Figure 19a). For the evaluation of the polymer electrolyte membrane, only the low frequency regime (below 20 kHz) is typically considered.[46–48] A detailed view of this regime is provided in Figure 19b. The data feature a first intersection with the x-axis around 47.3 kΩ, corresponding to ohmic

losses, followed by two semicircles and another intersection with the real axis at frequencies lower than 1 Hz. The data can be fitted reasonably well by an equivalent circuit depicted in the inset. Most importantly, the membrane (i.e. iCVD film) resistance can be determined from the intersection at higher frequencies (around 10 kHz).[23,48,49]

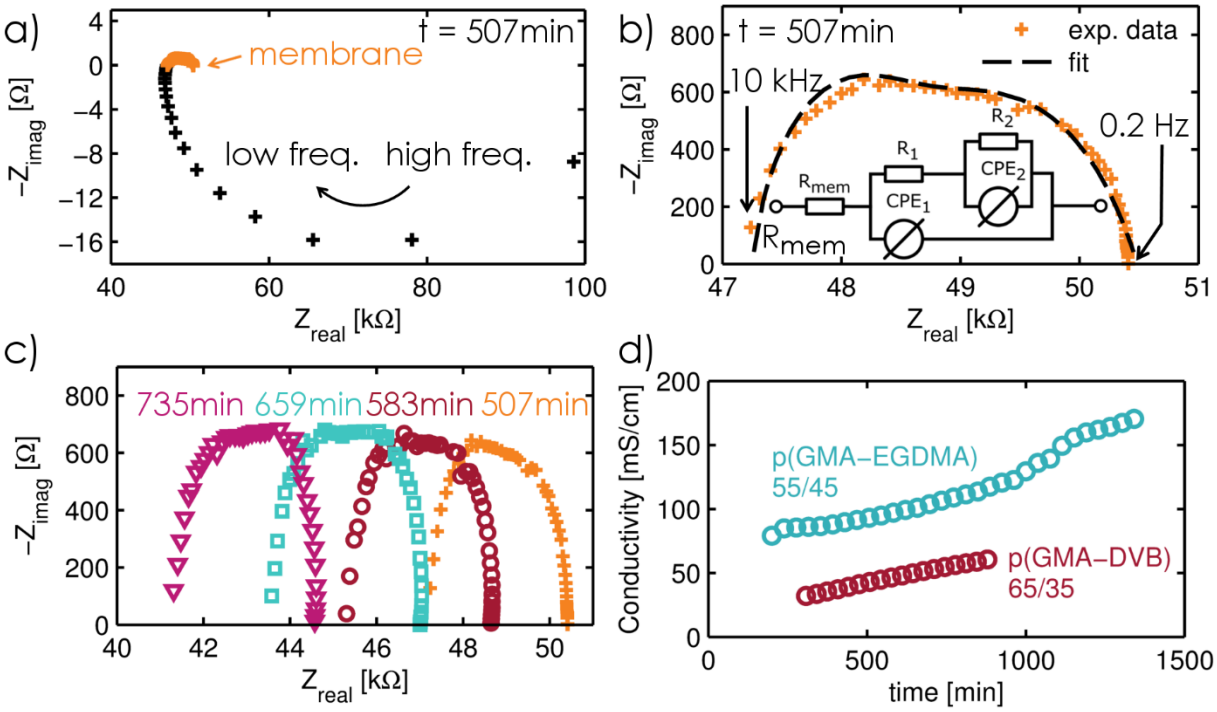

Figure 19. Electrochemical impedance spectroscopy data of a p(GMA-EGDMA) sample with 55 % GMA content. The data were collected in a closed system at saturated humidity. a) Nyquist plot of the full impedance spectrum collected after 507 seconds, depicting setup and membrane contributions. b) Nyquist plot of the membrane data. The inset depicts the equivalent circuit used in the fits. c) Selected impedance spectra depicting the change in impedance over time. d) Changes in conductivity of the iCVD film as a function of time. For comparison, data for a p(GMA-DVB) film with 65 % GMA content are also shown. Please note that conductivity values are calculated with the dry, as-deposited film thickness.

The two parallel RCs, on the other hand, could not be unambiguously interpreted but might be related to double layer formation or transport phenomena. In Figure 19c, impedance spectra at selected times are depicted, evidencing a shift of the total spectrum towards lower x-values. This means that the membrane resistance decreases gradually as the hydration level increases in the films. As the hydrated state is necessary for the dissociation of protons from the sulfonic acid groups, this behavior is expected. In Figure 19d, membrane conductivities are plotted as a function of time. Please note that these values are calculated with the thickness of the dry iCVD layers as the swollen thicknesses were experimentally not accessible. Therefore, values

represent an upper estimate of the true conductivity. The data show conductivity values of about 100 mS/cm, which is very promising for future experiments. As the curve does not show a saturation behavior, the apparent conductivity increase might be in fact related to further water uptake. As a constant thickness is assumed in the conductivity calculation, thickness changes induced by swelling are left unaccounted for. Nevertheless, this thickness increase should not surpass 100 %, meaning that the true membrane conductivity should still be in the order of 10 to 100 mS/cm. For comparison, also data for a polymer cross-linked with DVB are shown. While the slightly increased GMA content (65 compared to 55 %) suggests higher conductivities, data show actually the opposite behavior. A possible reason might be that DVB, in contrast to EGDMA, is highly rigid, possibly limiting chain rearrangement and charge transport.

Conclusion and outlook

The possibility to employ oxidative and initiated Chemical Vapor Deposition in the preparation of proton conductive membranes was investigated. The attempt to prepare poly(p-phenylene oxide) by oCVD was not successful in the investigated parameter range, indicating that this catalytic reaction is likely not feasible from the vapor phase. In a different approach, glycidyl methacrylate co-polymers were prepared by iCVD for subsequent sulfonation. For this, different cross-linkers and co-monomers were evaluated. While it was possible to sulfonate vapor-deposited polymers, delamination and other structural instabilities were commonly encountered in the films during the reaction. Exchanging the rigid silicon substrates with flexible polymeric ones (such as PET or nylon) did significantly enhance the film stability on the substrate. The increased surface area (due to roughness) and the flexibility of the support decrease the stress at the iCVD polymer/substrate interface when films turn hydrophilic (and thus start swelling) during sulfonation. Preliminary data from conductivity measurements by electrochemical impedance spectroscopy show promising values, with samples reaching conductivity values in the order of 10 to 100 mS/cm. While the experimental conditions do not yet allow for the deposition of thicker membranes within reasonable time/costs, such membranes could be interesting for small-scale applications such as in enzyme fuel cells. In a next step, the proton conductivities of such membranes need to be investigated as a function of polymer composition and further improvements in deposition speed and polymer stability need to be made. Ultimately, the goal will be to test these polymers in a demonstrational power device.

Acknowledgements

I am deeply indebted and uttermost grateful to Prof. Karen Gleason for giving me the chance to work in her lab. Always truly interested in my ongoing work and taking the time to discuss experimental progress in great detail, she provided me with new insights and invaluable advice. Rarely, if at all, have I learned so much in such short time! Thank you so much for making this great experience possible!

I would like to thank Junjie Zhao and Minghui Wang, who helped me to greatly expand my chemistry knowledge and who were always eager to discuss and give input on my experimental work.

I am thankful to Priya Moni, who introduced me to life at MIT (and G-Lab in particular), but also taught me how to operate the oCVD systems. Always being supportive, she helped me getting started in the lab and was always there to answer any of my questions.

I am most grateful to Andong Liu, with whom I spent many hours while working late night at the Institute for Soldier Nanotechnolgy (ISN). Not only did he introduce me to the iCVD reactors in the G-Lab and discussed with me reactor design in great detail, but he became also dear friend.

It was a pleasure to work, discuss and share an office with Xiouxiou Wang, Do Han Kim and Stefan Schröder. Thank you all for letting me be part of the great G-lab community and making me feel so welcome!

Last but not least, I am grateful to Alberto Perrotta for the insightful discussions about the interpretation of electrochemical impedance spectroscopy data.

Bibliography

(1) Mehta, V.; Cooper, J. S. Review and Analysis of PEM Fuel Cell Design and Manufacturing. *J. Power Sources* **2003**, *114* (1), 32–53.

(2) Neburchilov, V.; Martin, J.; Wang, H.; Zhang, J. A Review of Polymer Electrolyte Membranes for Direct Methanol Fuel Cells. *J. Power Sources* **2007**, *169* (2), 221–238.

(3) Peighambardoust, S. J.; Rowshanzamir, S.; Amjadi, M. Review of the Proton Exchange Membranes for Fuel Cell Applications. *Int. J. Hydrog. Energy* **2010**, *35* (17), 9349–9384.

(4) Wu, J.; Yuan, X. Z.; Martin, J. J.; Wang, H.; Zhang, J.; Shen, J.; Wu, S.; Merida, W. A Review of PEM Fuel Cell Durability: Degradation Mechanisms and Mitigation Strategies. *J. Power Sources* **2008**, *184* (1), 104–119.

(5) Hickner, M. A.; Ghassemi, H.; Kim, Y. S.; Einsla, B. R.; McGrath, J. E. Alternative Polymer Systems for Proton Exchange Membranes (PEMs). *Chem. Rev.* **2004**, *104* (10), 4587–4612.

(6) Poppe, D.; Frey, H.; Kreuer, K. D.; Heinzel, A.; Mülhaupt, R. Carboxylated and Sulfonated Poly(Arylene-Co-Arylene Sulfone)s: Thermostable Polyelectrolytes for Fuel Cell Applications. *Macromolecules* **2002**, *35* (21), 7936–7941.

(7) Bose, S.; Kuila, T.; Nguyen, T. X. H.; Kim, N. H.; Lau, K.; Lee, J. H. Polymer Membranes for High Temperature Proton Exchange Membrane Fuel Cell: Recent Advances and Challenges. *Prog. Polym. Sci.* **2011**, *36* (6), 813–843.

(8) Zhang, L.; Zhou, M.; Wen, D.; Bai, L.; Lou, B.; Dong, S. Small-Size Biofuel Cell on Paper. *Biosens. Bioelectron.* **2012**, *35* (1), 155–159.

(9) Coclite, A. M.; Lund, P.; Di Mundo, R.; Palumbo, F. Novel Hybrid Fluoro-Carboxylated Copolymers Deposited by Initiated Chemical Vapor Deposition as Protonic Membranes. *Polymer* **2013**, *54* (1), 24–30.

(10) Ranacher, C.; Resel, R.; Moni, P.; Cermenek, B.; Hacker, V.; Coclite, A. M. Layered Nanostructures in Proton Conductive Polymers Obtained by Initiated Chemical Vapor Deposition. *Macromolecules* **2015**, *48* (17), 6177–6185.

(11) Christian, P.; Coclite, A. M. Thermal Studies on Proton Conductive Copolymer Thin Films Based on Perfluoroacrylates Synthesized by Initiated Chemical Vapor Deposition. *Thin Solid Films* **2017**, *635* (Supplement C), 3–8.

(12) Mauritz, K. A.; Moore, R. B. State of Understanding of Nafion. *Chem. Rev.* **2004**, *104* (10), 4535–4586.

(13) Lee, W.; Shibasaki, A.; Saito, K.; Sugita, K.; Okuyama, K.; Sugo, T. Proton Transport Through Polyethylene-Tetrafluoroethylene-Copolymer-Based Membrane Containing Sulfonic Acid Group Prepared by RIGP. *J. Electrochem. Soc.* **1996**, *143* (9), 2795–2799.

(14) Buchmüller, Y.; Wokaun, A.; Gubler, L. Fuel Cell Membranes Based on Grafted and Post-Sulfonated Glycidyl Methacrylate (GMA). *Fuel Cells* **2013**, *13* (6), 1177–1185.

(15) Bakker, R.; Verlaan, V.; van der Werf, C. H. M.; Rath, J. K.; Gleason, K. K.; Schropp, R. E. I. Initiated Chemical Vapour Deposition (ICVD) of Thermally Stable Poly-Glycidyl Methacrylate. *Surf. Coat. Technol.* **2007**, *201* (22–23), 9422–9425.

(16) Tenhaeff, W. E.; Gleason, K. K. Initiated and Oxidative Chemical Vapor Deposition of Polymeric Thin Films: ICVD and OCVD. *Adv. Funct. Mater.* **2008**, *18* (7), 979–992.

(17) Vaddiraju, S.; Seneca, K.; Gleason, K. K. Novel Strategies for the Deposition of -COOH Functionalized Conducting Copolymer Films and the Assembly of Inorganic Nanoparticles on Conducting Polymer Platforms. *Adv. Funct. Mater.* **2008**, *18* (13), 1929–1938.

(18) Bhattacharyya, D.; Howden, R. M.; Borrelli, D. C.; Gleason, K. K. Vapor Phase Oxidative Synthesis of Conjugated Polymers and Applications. *J. Polym. Sci. Part B Polym. Phys.* **2012**, *50* (19), 1329–1351.

(19) Im, S. G.; Kusters, D.; Choi, W.; Baxamusa, S. H.; van de Sanden, M. C. M.; Gleason, K. K. Conformal Coverage of Poly(3,4-Ethylenedioxythiophene) Films with Tunable Nanoporosity via Oxidative Chemical Vapor Deposition. *ACS Nano* **2008**, *2* (9), 1959–1967.

(20) Goktas, H.; Wang, X.; D. Boscher, N.; Torosian, S.; K. Gleason, K. Functionalizable and Electrically Conductive Thin Films Formed by Oxidative Chemical Vapor Deposition (OCVD) from Mixtures of 3-Thiopheneethanol (3TE) and Ethylene Dioxythiophene (EDOT). *J. Mater. Chem. C* **2016**, *4* (16), 3403–3414.

(21) Xu, T.; Wu, D.; Wu, L. Poly(2,6-Dimethyl-1,4-Phenylene Oxide) (PPO)—A Versatile Starting Polymer for Proton Conductive Membranes (PCMs). *Prog. Polym. Sci.* **2008**, *33* (9), 894–915.

(22) Hay, A. S. Polymerization by Oxidative Coupling: Discovery and Commercialization of PPO® and Noryl® Resins. *J. Polym. Sci. Part Polym. Chem.* **1998**, *36* (4), 505–517.

(23) Zhang, J.; Zhang, H.; Wu, J.; Zhang, J. Chapter 5 - Membrane/Ionomer Proton Conductivity Measurements. In *Pem Fuel Cell Testing and Diagnosis*; Zhang, J., Zhang, H., Wu, J., Zhang, J., Eds.; Elsevier: Amsterdam, 2013; pp 143–170.

(24) H. Baxamusa, S.; Gap Im, S.; K. Gleason, K. Initiated and Oxidative Chemical Vapor Deposition : A Scalable Method for Conformal and Functional Polymer Films on Real Substrates. *Phys. Chem. Chem. Phys.* **2009**, *11* (26), 5227–5240.

(25) Coclite, A. M.; Howden, R. M.; Borrelli, D. C.; Petruczok, C. D.; Yang, R.; Yagüe, J. L.; Ugur, A.; Chen, N.; Lee, S.; Jo, W. J.; Liu, A.; Wang, X.; Gleason, K. K. 25th

Anniversary Article: CVD Polymers: A New Paradigm for Surface Modification and Device Fabrication. *Adv. Mater.* **2013**, *25* (38), 5392–5423.

(26) Gleason, K. K. *CVD Polymers: Fabrication of Organic Surfaces and Devices*; John Wiley & Sons, 2015.

(27) Lock, J. P.; Im, S. G.; Gleason, K. K. Oxidative Chemical Vapor Deposition of Electrically Conducting Poly(3,4-Ethylenedioxythiophene) Films. *Macromolecules* **2006**, *39* (16), 5326–5329.

(28) Higashimura, H.; Kobayashi, S. Oxidative Polymerization. In *Encyclopedia of Polymer Science and Technology*; John Wiley & Sons, Inc., 2002.

(29) Gupta, M.; Kapur, V.; Pinkerton, N. M.; Gleason, K. K. Initiated Chemical Vapor Deposition (ICVD) of Conformal Polymeric Nanocoatings for the Surface Modification of High-Aspect-Ratio Pores. *Chem. Mater.* **2008**, *20* (4), 1646–1651.

(30) Christian, P.; Coclite, A. M. Vapor-Phase-Synthesized Fluoroacrylate Polymer Thin Films: Thermal Stability and Structural Properties. *Beilstein J. Nanotechnol.* **2017**, *8* (1), 933–942.

(31) Lau, K. K. S.; Gleason, K. K. Initiated Chemical Vapor Deposition (ICVD) of Poly(Alkyl Acrylates): A Kinetic Model. *Macromolecules* **2006**, *39* (10), 3695–3703.

(32) Lin, B.; Cheng, S.; Qiu, L.; Yan, F.; Shang, S.; Lu, J. Protic Ionic Liquid-Based Hybrid Proton-Conducting Membranes for Anhydrous Proton Exchange Membrane Application. *Chem. Mater.* **2010**, *22* (5), 1807–1813.

(33) Miyake, H. The Design and Development of Flemion Membranes. In *Modern Chlor-Alkali Technology*; Wellington, T. C., Ed.; Springer Netherlands, 1992; pp 59–67.

(34) Bozkurt, A.; Meyer, W. H.; Gutmann, J.; Wegner, G. Proton Conducting Copolymers on the Basis of Vinylphosphonic Acid and 4-Vinylimidazole. *Solid State Ion.* **2003**, *164* (3–4), 169–176.

(35) Yang, R.; Xu, J.; Ozaydin-Ince, G.; Wong, S. Y.; Gleason, K. K. Surface-Tethered Zwitterionic Ultrathin Antifouling Coatings on Reverse Osmosis Membranes by Initiated Chemical Vapor Deposition. *Chem. Mater.* **2011**, *23* (5), 1263–1272.

(36) Glycidyl Methacrylate SAFETY DATA SHEET. Sigma-Aldrich Corporation November 15, 2017.

(37) Liland, K. H.; Mevik, B.-H.; Canteri, R. *Baseline: Baseline Correction of Spectra. R Package Version 1.2-0*; 2015.

(38) Nečas, D.; Klapetek, P. Gwyddion: An Open-Source Software for SPM Data Analysis. *Cent. Eur. J. Phys.* **2011**, *10* (1), 181–188.

(39) Ferric chloride - CAMEO http://cameo.mfa.org/wiki/Ferric_chloride (accessed Oct 6, 2017).

(40) Hay, A. S.; Blanchard, H. S.; Endres, G. F.; Eustance, J. W. POLYMERIZATION BY OXIDATIVE COUPLING. *J. Am. Chem. Soc.* **1959**, *81* (23), 6335–6336.

(41) Tsuchida, E.; Kaneko, M.; Nishide, H. The Kinetics of the Oxidative Polymerization of 2.6-xylenol with a Copper-amine Complex. *Macromol. Chem. Phys.* **1972**, *151* (1), 221–234.

(42) Morosin, B. Structure Refinements on Dichloro- and Dibromobis(Pyridine)Copper(II). *Acta Crystallogr. B* **1975**, *31* (2), 632–634.

(43) Larkin, P. *Infrared and Raman Spectroscopy: Principles and Spectral Interpretation*; Elsevier, 2011.

(44) Bondar, Y. V.; Kim, H. J.; Lim, Y. J. Sulfonation of (Glycidyl Methacrylate) Chains Grafted onto Nonwoven Polypropylene Fabric. *J. Appl. Polym. Sci.* **2007**, *104* (5), 3256–3260.

(45) Tazreiter, M.; Christian, P.; Schennach, R.; Grießer, T.; Maria Coclite, A. Simple Method for the Quantitative Analysis of Thin Copolymer Films on Substrates by Infrared Spectroscopy Using Direct Calibration. *Anal. Methods* **2017**.

(46) Asghari, S.; Mokmeli, A.; Samavati, M. Study of PEM Fuel Cell Performance by Electrochemical Impedance Spectroscopy. *Int. J. Hydrog. Energy* **2010**, *35* (17), 9283–9290.

(47) Sun, S.; Xiao, Y.; Liang, D.; Shao, Z.; Yu, H.; Hou, M.; Yi, B. Behaviors of a Proton Exchange Membrane Electrolyzer under Water Starvation. *RSC Adv.* **2015**, *5* (19), 14506–14513.

(48) Feketeföldi, B.; Cermenek, B.; Spirk, C.; Alex; Schenk, E.; Grimmer, C.; Bodner, M.; Koller, M.; Ribitsch, V.; Hacker, V. Chitosan-Based Anion Exchange Membranes for Direct Ethanol Fuel Cells. *J. Membr. Sci. Technol.* **2016**, 6 (1).

(49) Bodner, M.; Cermenek, B.; Rami, M.; Hacker, V. The Effect of Platinum Electrocatalyst on Membrane Degradation in Polymer Electrolyte Fuel Cells. *Membranes* **2015**, *5* (4), 888–902.